2024 European Control Conference (ECC)
June 25-28, 2024. Stockholm, Sweden

Sensitivity-based moving horizon estimation of road friction*

Fadi Snobar[1], Andreas Michalka[1], Maik Horn[2], Christoph Strohmeyer[2], and Knut Graichen[1]

Abstract— **Environmental factors such as rain, snow, or ice significantly impact road friction, which correlates strongly with traffic safety. This work uses a sensitivity-based moving horizon estimator to gauge the maximum road friction coefficient online. The adopted friction estimation strategy combines the estimated rack force based on a linear steering system model with a nonlinear two-degree-of-freedom (DoF) single-track vehicle model. The parametric output sensitivity is monitored and integrated within the moving horizon estimation (MHE) framework to prevent an arbitrary estimate in the absence of sufficient excitation. The method is evaluated by simulations and experiments under various road conditions. The results validate the proposed strategy and demonstrate its capability to reliably estimate the maximum road friction coefficient.**

I. Introduction

Empirical data shows a strong correlation between road friction and traffic safety [1]. Environmental factors such as rain, snow, or ice significantly impact road friction. Despite drivers adjusting their behavior depending on environmental factors, road appearance is only sometimes a reliable indicator of friction, and conditions such as ice on the road may not be clearly visible.

The so-called maximum road friction coefficient is essential for any onboard control device relying on a car model, e.g., stability control, and trajectory or path planning for autonomous vehicles, necessitating its precise real-time estimation. The maximum road friction quantifies the grip limit between the tires and the road. Because this study only considers vehicle lateral dynamics, the maximum road friction is defined as $\mu = \max |^{F_{\mathrm{f},y}}/_{F_{\mathrm{f},z}}|$, where $F_{\mathrm{f},y}$ and $F_{\mathrm{f},z}$ are the lateral and normal forces on the front axle, respectively. Maximum road friction coefficient assessment can be categorized into cause-based and effect-based methods [2]. The former determines road friction by its physical cause, for instance, material, tire depth, temperature, etc. Effect-based methods, however, deduce road friction from tire response. One such response is the slip angle, which is the focus of this paper.

Slip-angle-based methods of estimating the maximum road friction coefficient have been the core subject of many studies. In [3] and [2], the longitudinal slip has been used to estimate road friction during longitudinal acceleration or braking. On the other hand, [4], [5], [6] rely on lateral slip to estimate road friction when the vehicle steers. These papers employ the self-aligning torque (SAT) to estimate the friction coefficient at lower excitation levels than when using lateral acceleration. The SAT, however, is difficult to measure and, therefore, to validate. A combination of lateral and longitudinal vehicle models can be found in [7], where the road friction is estimated using an unscented Kalman filter (UKF) with a 13-degree-of-freedom (DoF) vehicle model in combination with local sensitivity analysis to avoid estimation drift.

Many approaches in the literature rely on extensive knowledge of the tires and vehicle dynamics to estimate the maximum road friction coefficient μ. However, large models with many parameters are computationally costly and vulnerable to parameter changes. In this paper, a novel sensitivity-based moving horizon estimation (MHE) of the road friction is developed based on a two-DoF nonlinear single-track model. A benefit of MHE over Kalman filtering is the ability to encompass constraints and to tailor the cost function to be minimized to the specific application. The general operating principle is depicted in Fig. 1. Measurements of the vehicle are used by a rack force estimator that provides the rack force as an additional measurement to the subsequent state and friction estimator block. Similar to SAT, the rack force allows estimating the maximum road friction at lower excitation levels than solely relying on lateral acceleration and yaw rate. In contrast to SAT, however, the rack force can be quite easily measured using strain gauge sensors, allowing for more straightforward validation. The subsequent state and friction estimator block in Fig. 1 basically consists of two moving-horizon-based state and friction estimators. To avoid an arbitrary road friction estimation without sufficient excitation, i.e., in instances of low identifiability, the sensitivities of the outputs to road friction are monitored. In light of this, the μ-update is slowed down or even stopped when the sensitivity is too low. The sensitivity is assessed within the whole optimization horizon of the MHE instead of at a single time instant, which would be the case for a Kalman-filter-based parameter estimation, providing higher robustness against noise.

The remainder of the paper is structured as follows: the rack force estimation with a linear steering system model and moving-horizon-based vehicle state estimation with a nonlinear single-track model are introduced in Section II. The maximum road friction estimation algorithm and the sensitivity analysis are described in Section III. Finally, the maximum road friction estimator is validated in Section IV using simulations as well as experimental data from a test rig and a vehicle driving on dry and wet asphalt.

*This work has been supported by the Schaeffler Hub for Advanced Research at Friedrich-Alexander-Universtät Erlangen-Nürnberg (SHARE at FAU).

[1]Chair of Automatic Control, Friedrich-Alexander-Universität Erlangen-Nürnberg, Erlangen, Germany, fadi.snobar@fau.de, andreas.michalka@fau.de, knut.graichen@fau.de

[2]Schaeffler Technologies AG & Co. KG, Herzogenaurach, Germany, maik.horn@schaeffler.com, christoph.strohmeyer@schaeffler.com

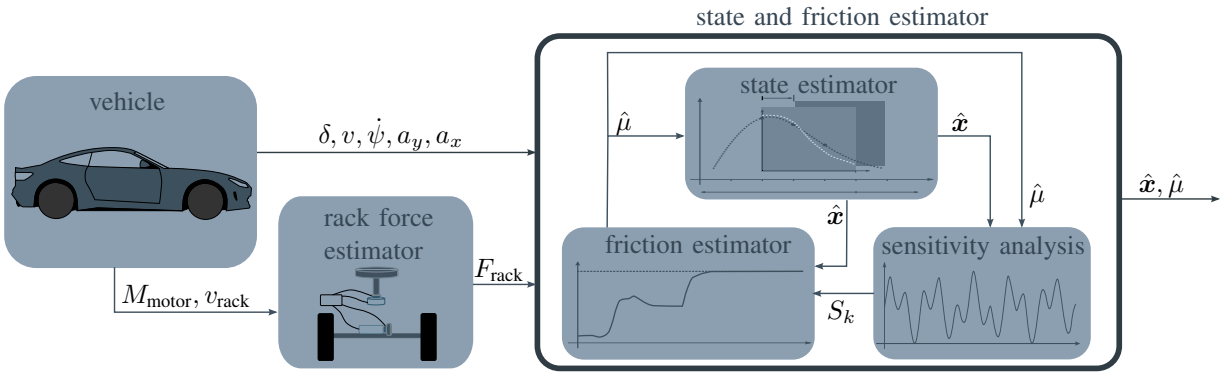

Fig. 1: Block diagram of sensitivity-based moving horizon estimation of road friction.

II. Rack force and state estimation

Determining the rack force can be done in two ways: either by modeling the car's lateral dynamics as previously done in [8] or by modeling the steering system when there is access to the road wheel actuator current or torque. The following section provides a brief overview of rack force estimation with a linear steering model. Additionally, the moving horizon-based state estimator in Fig. 1 is described using a nonlinear vehicle model. In the context of MHE, the estimated rack force is used as an additional measurement, which should increase the accuracy of the state estimation and allow for friction estimation at lower excitation than when solely relying on the lateral acceleration and yaw rate. This is because the rack force reaches its maximum at lower slip angles than the lateral force, as shown later in Section II-B.

A. Rack force estimation

A common way of estimating the rack force involves utilizing the steering system. To this end, the steering system is modeled as a single mass system given by

$$m_{\text{rack}}\dot{v}_{\text{rack}} = \frac{iM_{\text{motor}}}{r} - F_{\text{rack}}, \tag{1}$$

where $F_{\text{rack}}, v_{\text{rack}}$, and m_{rack} represent the rack force, rack velocity, and combined mass of the rack, respectively. The friction force is assumed to be negligible. The motor torque exerted on the steering rack is M_{motor}, i is the transmission ratio and r is the length of the lever arm. Similar models can be found, e.g, in [9] and [10]. Note that a steer-by-wire (SbW) system is considered in this paper, ergo the force applied by the driver on the steering wheel does not transfer directly to the rack. With the road wheel actuator torque as the input, the measured rack speed as the output, and the rack force as disturbance, the state-space formulation of the steering system results in

$$\begin{bmatrix}\dot{v}_{\text{rack}}\\ \dot{F}_{\text{rack}}\end{bmatrix} = \begin{bmatrix}0 & -\frac{1}{m_{\text{rack}}}\\ 0 & 0\end{bmatrix}\begin{bmatrix}v_{\text{rack}}\\ F_{\text{rack}}\end{bmatrix} + \begin{bmatrix}\frac{i}{m_{\text{rack}}r}\\ 0\end{bmatrix} M_{\text{motor}} \tag{2a}$$

$$y = \begin{bmatrix}1 & 0\end{bmatrix}\begin{bmatrix}v_{\text{rack}}\\ F_{\text{rack}}\end{bmatrix}. \tag{2b}$$

The state-space formulation (2) is used for a linear Kalman-Bucy filter. An example of the estimation result is illustrated in Fig. 2, corresponding to a normalized root-mean-square error (NRMSE)* of 3.7 %. The small error shows the capability of this method in spite of its simplicity.

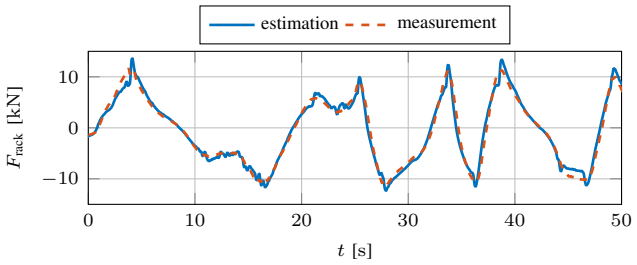

Fig. 2: Rack force measurement and estimation.

B. Moving-horizon-based vehicle state estimation

The lateral dynamics of the vehicle can be described by a two-DoF single-track model with the lateral forces $F_{\text{f},y}$ and $F_{\text{r},y}$ acting on the front and rear axle, see Fig. 3. The parameters l_{f} and l_{r} indicate the distance from the center of gravity (CoG) to the front and rear axles. The absolute velocity of the vehicle is denoted by v, the steer angle by δ, the side-slip angle by β, and the yaw rate by $\dot{\psi}$. Based on [11], [12], and by neglecting the longitudinal forces acting on the tires, the equations of motion for the nonlinear single-track model result in

$$\begin{bmatrix}\dot{\beta}\\ \ddot{\psi}\end{bmatrix} = \begin{bmatrix}-\dot{\psi} + \frac{1}{mv}\left(F_{\text{f},y}\cos\left(\delta-\beta\right) + F_{\text{r},y}\cos\left(\beta\right)\right)\\ \frac{1}{I_{zz}}\left(F_{\text{f},y}\cos\left(\delta\right)l_{\text{f}} - F_{\text{r},y}l_{\text{r}}\right)\end{bmatrix}, \tag{3}$$

where I_{zz} is the moment of inertia about the z_{v}-axis.

The lateral forces $F_{i,y}$ with $i \in \{\text{f},\text{r}\}$ depend on the front and rear slip angles α_i, i.e., the angle between the longitudinal axis of the respective tire and its direction of motion, cf. Fig. 3. Using geometric considerations, α_{f} and

*NRMSE $= \frac{\sqrt{\frac{1}{n}\sum_{k=1}^{n}(y_k-\hat{y}_k)^2}}{y_{\max}-y_{\min}}$, where n is the number of observations.

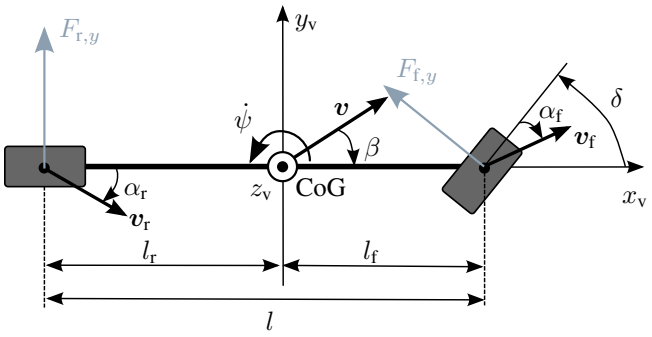

Fig. 3: Single-track model.

α_r can be expressed as

$$\alpha_\mathrm{f} = \delta - \arctan\left(\frac{v\sin\beta + l_\mathrm{f}\dot{\psi}}{v\cos\beta}\right) \tag{4a}$$

$$\alpha_\mathrm{r} = -\arctan\left(\frac{v\sin\beta - l_\mathrm{r}\dot{\psi}}{v\cos\beta}\right). \tag{4b}$$

A tire model is necessary to characterize the lateral forces $F_{i,y}$. This work employs an exponential tire model [13]

$$F_{i,y} = \mu F_{i,z}\left(1 - e^{-K|\alpha_i|}\right)\operatorname{sign}(\alpha_i), \quad i \in \{\mathrm{f},\mathrm{r}\}, \tag{5}$$

where μ is the maximum lateral coefficient of friction between the tire and the road and $F_{i,z}$ denotes the normal forces acting on the front and rear tires. Additionally, K is related to the cornering stiffness C_α of the tires, which determines the slope of the curve for small slip angles α_i. The normal forces $F_{i,z}$ are modeled using quasi-static load distribution, taking into account the longitudinal acceleration a_x and the height h of the CoG above the ground, i.e.,

$$F_{\mathrm{f},z} = m\frac{-a_x h + g l_\mathrm{r}}{l_\mathrm{f} + l_\mathrm{r}}, \quad F_{\mathrm{r},z} = m\frac{a_x h + g l_\mathrm{f}}{l_\mathrm{f} + l_\mathrm{r}}. \tag{6}$$

Using the lateral force on the front tire $F_{\mathrm{f},y}$, the rack force can be expressed as

$$F_\mathrm{rack} = F_{\mathrm{f},y}(t_\mathrm{m} + t_\mathrm{p}(\alpha_\mathrm{f}))i_\mathrm{p} = M_\mathrm{align} i_\mathrm{p}, \tag{7}$$

where t_m and $t_\mathrm{p}(\alpha_\mathrm{f})$ denote the mechanical and pneumatic trails, and i_p is the ratio between the self-aligning torque M_align and the corresponding rack force for the given vehicle. The pneumatic trail $t_\mathrm{p}(\alpha_\mathrm{f})$ is modeled according to [6] as a linearly decreasing function of $\tan(\alpha_\mathrm{f})$, while t_m is assumed to be constant. In Fig. 4, a comparison between (5) and (7) is depicted. The comparison illustrates that F_rack reaches its maximum at lower slip angles α_f, indicating lower excitation levels compared to $F_{\mathrm{f},y}$.

The overall single-track model (3) with the slip angles (4), tire model (5), and normal forces (6) can be represented as a nonlinear state-space model $\dot{\boldsymbol{x}} = \boldsymbol{f}(\boldsymbol{x}, \boldsymbol{u}, \mu, t)$ with the state and control vectors

$$\boldsymbol{x} = \begin{bmatrix}\beta & \dot{\psi}\end{bmatrix}^\mathsf{T}, \quad \boldsymbol{u} = \begin{bmatrix}v & \delta & a_x\end{bmatrix}^\mathsf{T}. \tag{8}$$

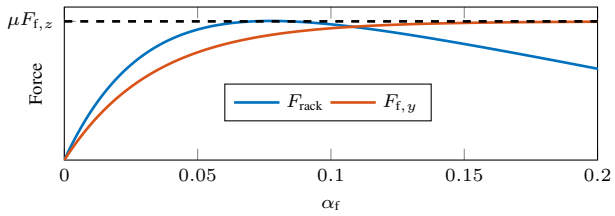

Fig. 4: Front lateral force $F_{\mathrm{f},y}$ and rack force F_rack plotted over the slip angle α_f.

The output measurements of the system consist of the lateral acceleration, the yaw rate, and the rack force computed in Section II-A, i.e.,

$$\boldsymbol{y} = \boldsymbol{h}(\boldsymbol{x}, \boldsymbol{u}, \mu) = \begin{bmatrix} a_y \\ \dot{\psi} \\ \hat{F}_\mathrm{rack} \end{bmatrix} = \begin{bmatrix} \frac{1}{m}(F_{\mathrm{f},y}\cos\delta + F_{\mathrm{r},y}) \\ \dot{\psi} \\ M_\mathrm{align} i_\mathrm{p} \end{bmatrix}. \tag{9}$$

The state vector $\boldsymbol{x}$ is estimated using MHE, a nonlinear optimization-based method. MHE aims to find the optimal state trajectory $\boldsymbol{x}^*(t_k - T, t_k)$ that minimizes a cost functional J over the recent past horizon $T > 0$ for each time step $t_k = t_0 + k\Delta t$ with the sampling time $\Delta t > 0$. The MHE problem is formulated as

$$\min_{\hat{\boldsymbol{x}}_k} \quad J(\hat{\boldsymbol{x}}_k, \hat{\mu}_k, \boldsymbol{Q}) = \int_{t_k - T}^{t_k} \Delta\boldsymbol{y}(t)^\mathsf{T}\boldsymbol{Q}\Delta\boldsymbol{y}(t)\ \mathrm{d}t \tag{10a}$$

$$\text{s.t.} \quad \dot{\boldsymbol{x}} = \boldsymbol{f}(\boldsymbol{x}(t), \bar{\boldsymbol{u}}(t), \hat{\mu}_k, t), \quad \boldsymbol{x}(t_k) = \hat{\boldsymbol{x}}_k \tag{10b}$$

$$\boldsymbol{y} = \boldsymbol{h}(\boldsymbol{x}(t), \bar{\boldsymbol{u}}(t), \hat{\mu}_k) \tag{10c}$$

$$\boldsymbol{x} \in X = [\boldsymbol{x}_\mathrm{min}, \boldsymbol{x}_\mathrm{max}], \tag{10d}$$

where $\boldsymbol{Q}$ is a positive semi-definite diagonal weighting matrix, $\bar{\boldsymbol{u}}(t)$ is the control vector, and $\Delta\boldsymbol{y}(t) = \boldsymbol{y} - \bar{\boldsymbol{y}}(t)$ with the measurements $\bar{\boldsymbol{y}}(t)$. Moreover, (10d) constitutes the box constraints for the states $\boldsymbol{x}$ to avoid state estimation in unreasonable domains. The estimated road friction coefficient $\hat{\mu}_k$ is determined in Section III. The toolbox GRAMPC [14] for nonlinear continuous-time systems was implemented to solve (10). More in-depth information on MHE can be found, e.g., in [15].

III. Road Friction Estimation

Estimating the maximum road friction coefficient μ is more delicate than the state estimation described above. In particular, the identifiability of μ strongly depends on the excitation level of the rack force F_rack. Therefore, the estimation of μ is handled as a separate problem, which would also provide the possibility of estimating μ and $\boldsymbol{x}$ with different time scales, if necessary.

A. Proximal minimization problem

By examining Fig. 4, it becomes apparent that an estimator can only determine the maximum road friction coefficient in the vicinity of either peak. In more technical terms, the parameter μ has low *identifiability* in regions away from the peaks. Consequently, estimating μ in areas of low identifiability would yield arbitrary results, meaning an estimator might be badly conditioned or converge to an element of

the set of local or global minima, depending on the initial conditions [16]. The parametric output sensitivity, discussed later in Section III-B, is taken as a measure of local at-point identifiability.

The maximum road friction coefficient μ is estimated by the proximal minimization problem

$$\hat{\mu}_{k+1} = \arg\min_{\hat{\mu}\in M} \Bigg(J(\hat{\boldsymbol{x}}_k, \hat{\mu}_k, \boldsymbol{Q}_\mu) + \int_{t_k - T_\mu}^{t_k} \frac{1}{2\gamma_k(S_k)} ||\hat{\mu} - \hat{\mu}_k||^2 \mathrm{d}t \Bigg), \tag{11}$$

encompassing the sensitivity-dependent weight $\gamma_k(S_k)$, introduced in Section III-B, as a measure of identifiability. The box constraint of the μ-estimate is $M = [\mu_{\min}, \mu_{\max}]$. A different weighting matrix $\boldsymbol{Q}_\mu$ than in (10) is chosen because, as mentioned earlier, the identifiability of μ strongly depends on the excitation level of the rack force. For the state estimation (10), however, the outputs are weighted similarly. The proximal minimization problem (11) is a compromise between the minimization of J and penalizing the distance to the previous iteration point with the sensitivity-dependent weight $\gamma_k(S_k)$. Under the assumption that the proximal minimization problem (11) is strictly convex, which holds if (10a) is strictly convex or if $\gamma_k(S_k)$ is sufficiently small, the solution is given by

$$\hat{\mu}_{k+1} = \psi\left(\hat{\mu}_k + \gamma_k(S_k) \nabla_\mu J(\hat{\boldsymbol{x}}_k, \hat{\mu}_k, \boldsymbol{Q}_\mu)\right) \tag{12}$$

with the projection function

$$\psi(\hat{\mu}_k) = \begin{cases} \mu_{\min} & \text{if } \hat{\mu}_k < \mu_{\min} \\ \mu_{\max} & \text{if } \hat{\mu}_k > \mu_{\max} \\ \hat{\mu}_k & \text{else} \end{cases} \tag{13}$$

to account for the constraint set $M = [\mu_{\min}, \mu_{\max}]$. The gradient of $J(\hat{\boldsymbol{x}}_k, \hat{\mu}_k, \boldsymbol{Q}_\mu)$ with respect to μ at the point $\hat{\mu}_k$ is given by

$$\nabla_\mu J(\hat{\boldsymbol{x}}_k, \hat{\mu}_k, \boldsymbol{Q}_\mu) = \int_{t_k - T_\mu}^{t_k} \frac{\partial}{\partial \mu} H(\hat{\boldsymbol{x}}_k, \boldsymbol{u}, \hat{\mu}_k, \boldsymbol{\lambda}) \, \mathrm{d}t \tag{14}$$

with the Hamiltonian

$$H(\hat{\boldsymbol{x}}_k, \boldsymbol{u}, \hat{\mu}_k, \boldsymbol{\lambda}) = \Delta \boldsymbol{y}^\mathsf{T} \boldsymbol{Q}_\mu \Delta \boldsymbol{y} + \boldsymbol{\lambda}^\mathsf{T} \boldsymbol{f}(\hat{\boldsymbol{x}}_k, \boldsymbol{u}, \hat{\mu}_k) \tag{15}$$

and the adjoint state vector $\boldsymbol{\lambda}(t), t \in [t_k - T, t_k]$ satisfying the adjoint dynamics

$$\dot{\boldsymbol{\lambda}} = -\frac{\partial H(\hat{\boldsymbol{x}}_k, \boldsymbol{u}, \hat{\mu}_k, \boldsymbol{\lambda})}{\partial \boldsymbol{x}}, \quad \boldsymbol{\lambda}(t_k) = 0, \tag{16}$$

which can be solved backward in time to obtain $\boldsymbol{\lambda}$. The state vector $\hat{\boldsymbol{x}}_k$ follows from (10b).

B. Sensitivity analysis

The local at-point identifiability within the optimization horizon of each time step is assessed to avoid the risk of an arbitrary μ-estimation. This is achieved with the help of *parametric output sensitivity*, which describes how sensitive the outputs are to parameter changes [17]. As the sensitivity of the outputs to perturbations in a particular parameter increases, the parameter becomes more critical to the system behavior.

Consider the first-order sensitivities of the state $\boldsymbol{x}_\mu(t) = {}^{\partial \boldsymbol{x}(t,\mu)}/_{\partial \mu}$ and the output $\boldsymbol{y}_\mu(t) = {}^{\partial \boldsymbol{y}(t,\mu)}/_{\partial \mu}$ with respect to μ. The corresponding dynamics follow from (10b) and (10c)

$$\frac{\mathrm{d}}{\mathrm{d}t}\boldsymbol{x}_\mu = \frac{\partial \boldsymbol{f}}{\partial \boldsymbol{x}}\boldsymbol{x}_\mu + \frac{\partial \boldsymbol{f}}{\partial \mu}, \quad \boldsymbol{x}_\mu(t_k - T) = \boldsymbol{x}_{\mu_0}, \tag{17a}$$

$$\boldsymbol{y}_\mu = \frac{\partial \boldsymbol{h}}{\partial \boldsymbol{x}}\boldsymbol{x}_\mu + \frac{\partial \boldsymbol{h}}{\partial \mu}. \tag{17b}$$

where $\boldsymbol{x}_{\mu 0} = \boldsymbol{x}_\mu(t_{k-1} - T_\mu + \Delta t)$ if $k > 0$ and $\boldsymbol{x}_{\mu 0} = \boldsymbol{0}$ if $k = 0$. Note that (17) is a linear time-varying system of differential equations. The sensitivity matrix $\boldsymbol{S}$ is then defined as

$$\boldsymbol{S} = \hat{\mu}_k \begin{bmatrix} \boldsymbol{y}_\mu(t_k - T) \cdot / \boldsymbol{y}(t_k - T) \\ \vdots \\ \boldsymbol{y}_\mu(t_k) \cdot / \boldsymbol{y}(t_k) \end{bmatrix} \tag{18}$$

where $\cdot/$ denotes element-wise vector division. The division and multiplication by $\boldsymbol{y}$ and $\hat{\mu}_k$ normalize the sensitivities to allow for better comparison between driving scenarios and road conditions. The recent past horizon T at each time instant t_k is discretized into N steps, therefore $\boldsymbol{S} \in \mathbb{R}^{3N \times 1}$. This matrix basically consists of snippets of the output sensitivities at each time instant within the optimization horizon. A scalar measure of the sensitivity can be computed as

$$S_k = \boldsymbol{S}^\mathsf{T} \boldsymbol{S}, \tag{19}$$

i.e., a sum of the normalized squared sensitivities of each output. Below a certain threshold $S_{\text{threshold}}$, the parameter μ is considered not locally identifiable since, within the given horizon, the parameter would have a negligible effect on the output.

The weight $\gamma_k(S_k)$ in the proximal minimization problem (11) is defined as

$$\gamma_k(S_k) = \frac{\gamma_{0,k}}{1 + e^{-c(S_k - S_{\text{threshold}})}} \tag{20}$$

to encompass the sensitivity into the update law (12), which is essentially a sigmoid function taking possible values between 0 and $\gamma_{0,k}$. The inflection point of the curve is given

Algorithm 1 Sensitivity-based MHE

1: **Initialize:**
   $\boldsymbol{x}_0, \mu_0$
2: **while** $t < T_{\text{sim}}$ **do**
3: compute $\hat{\boldsymbol{x}}_k$ from (10)
4: compute $\boldsymbol{x}_\mu$ and $\boldsymbol{y}_\mu$ in (17)
5: compute $\boldsymbol{S}$ and S_k using (18) and (19), respectively
6: compute (16) and (14) to get $\nabla_\mu J(\hat{\boldsymbol{x}}_k, \hat{\mu}_k, \boldsymbol{Q}_\mu)$
7: compute step size $\gamma_k(S_k)$ from (20)
8: compute μ_{k+1} using (12)
9: set $k \leftarrow k + 1$ and go to step 2
10: **end while**

by $S_{\text{threshold}}$, while c determines the gradient. Therefore, (20) modifies the step size in (12) depending on the sensitivity. Specifically, the step size is reduced in regions of low sensitivity to avoid false or untrustworthy predictions. The estimation method is summarized in Algorithm 1.

IV. Validation

The maximum road friction estimation scheme is validated with the help of simulations, a test rig, and finally, data from a vehicle on a test track. The latter was conducted on road surfaces with a variety of friction coefficients.

A. Simulation results

The estimation method is tested against a well-parameterized model in the simulation environment CarMaker*. The tests encompass different road friction coefficients.

Fig. 5a shows an example of the μ-estimation results using strong adaptation (——) with $c = 1$ in (20), weak adaptation (·····) with $c = 0.07$, and no adaptation with $c = 0$ (-·-·-). The outputs are plotted in Fig. 5c and Fig. 5d. At around $t \approx 13\,\text{s}$, all three estimators reach the correct value of μ when the excitation is high enough, i.e., $S > 40$, cf. Fig. 5b.

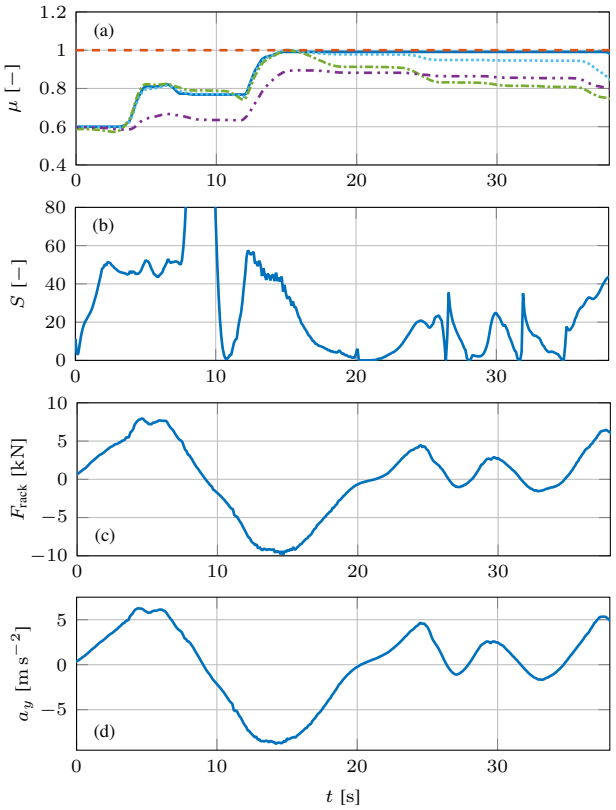

Fig. 5: Results using CarMaker simulation data: actual (– – –); strong adaptation $c = 1$ (——); weak adaptation $c = 0.07$ (·····); no adaptation $c = 0$ (-·-·-); without rack force measurement (-··-··-).

*https://ipg-automotive.com/en/products-solutions/software/carmaker/

However, in the case of no adaptation ($c = 0$) and when the sensitivity is low, the estimation presents a notable deviation from the actual value of the maximum road friction coefficient of 1.0. Conversely, exploiting the sensitivity illustrated in Fig. 5b by setting $c > 0$ slows down the update of μ as the sensitivity declines. The amount by which μ is updated when the sensitivity is close to $S_{\text{threshold}}$ depends on the tuning parameter c in (20), as depicted in Fig. 5a. Note that the impulse-like peaks in Fig. 5b correspond to zero-crossings due to the normalization in (18). As seen in the figure, the peaks do not notably affect the estimation, since (20) can only take values between 0 and $\gamma_{0,k}$.

In Section II, it was claimed that using the (estimated) rack force as an additional measurement would enable estimating road friction at lower slip angles α_{f}, thus requiring lower excitation levels compared to relying solely on lateral acceleration and yaw rate. To test this assertion, the road friction estimation without the rack force measurement (-··-··-) is depicted in Fig. 5a with $c = 0$. The figure shows that the estimated road friction does not reach the actual value of μ, even with high lateral accelerations well beyond $a_y = 5\,\text{m s}^{-2}$, thus validating the previously mentioned claim.

Another test scenario is illustrated in Fig. 6. At around $t = 3\,\text{s}$, μ changes abruptly from 1.0 (section ①) to 0.5 (section ②), as seen in Fig. 6a. A change in the μ-estimate is triggered when the sensitivity S increases, because at the time the actual value of μ changes the outputs illustrated in

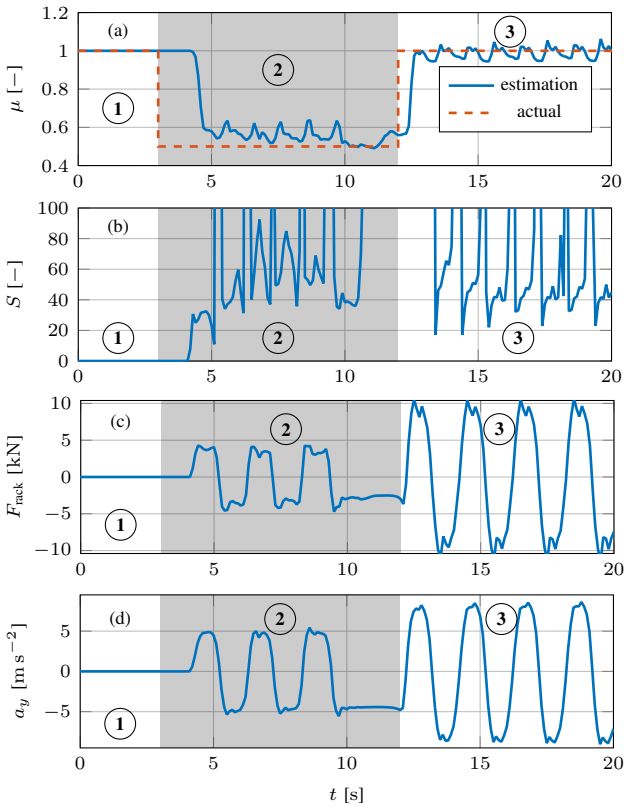

Fig. 6: Results using CarMaker simulation data with changing road friction coefficients.

Fig. 6c and Fig. 6d are equal to zero. At the transition from (2) to (3), i.e., when the road friction coefficient changes rapidly from 0.5 to 1.0, the μ-estimate is adjusted rapidly and reaches the correct value in around one second. Thus, one can discern that the method is equally suited for estimating rapid changes in μ.

B. Experimental results

The experimental validation was first conducted on a test rig and then on a vehicle operating on dry and wet tracks. The test rig simulates the car in CarMaker, then applies the computed lateral forces on an experimental configuration of the steering system, yielding simulated car data in combination with measured road wheel actuator torque. The results are depicted in Fig. 7a, which show that the estimation reaches the vicinity of the actual value of road friction, $\mu = 1.1$, when enough excitation is present, cf. Fig. 7b.

Additionally, a number of tests were carried out using data from a vehicle driving on dry and wet tracks. One example is shown in Fig. 8a, which exhibits a rapid change in μ at $t \approx 15.6\,\mathrm{s}$ due to the transition from a wet track to a dry one. According to [1], dry asphalt has a maximum road friction coefficient of $\mu \approx 0.8 - 1$, whereas on wet asphalt $\mu \approx 0.7 - 0.8$. On the wet track, starting with an initial $\mu_0 = 0.6$, the μ-estimate reaches the theoretical region between $0.7 - 0.8$ in the presence of sufficient excitation (see Fig. 8b). Analogously, the μ-estimate increases on the dry track until reaching a value within the theoretical range of $0.8 - 1.0$. Consistently with the simulation results in the previous section and owing to the sensitivity-based MHE, even when the sensitivity is low due to the excitation decreasing, as seen in Fig. 8b, the estimated μ is kept within the theoretical range. It is worth noting that for this test the direct measurement of the rack force was taken instead of the estimation because, at the time of writing, the motor torque M_{motor} in (2) of the test vehicle was not available.

V. Conclusions

The paper introduces an MHE scheme for simultaneously estimating the states of a two-DoF nonlinear single-track vehicle model and the maximum road friction coefficient. Firstly, a rack force estimator with a linear steering system model is presented. In addition, a representation of the lateral vehicle dynamics with an exponential tire model is introduced. This combined approach allows for estimation at lower excitation levels compared to the sole use of lateral dynamics. The MHE approach consists of a separate state and friction estimator in connection with a sensitivity analysis to prevent an arbitrary road friction estimation in the absence of sufficient excitation by adjusting the step size of the friction update accordingly. The results confirm that the developed method is well-suited for estimating maximum road friction. Further tests, tuning, and code optimization are necessary to ensure real-time feasibility on an onboard car computer.

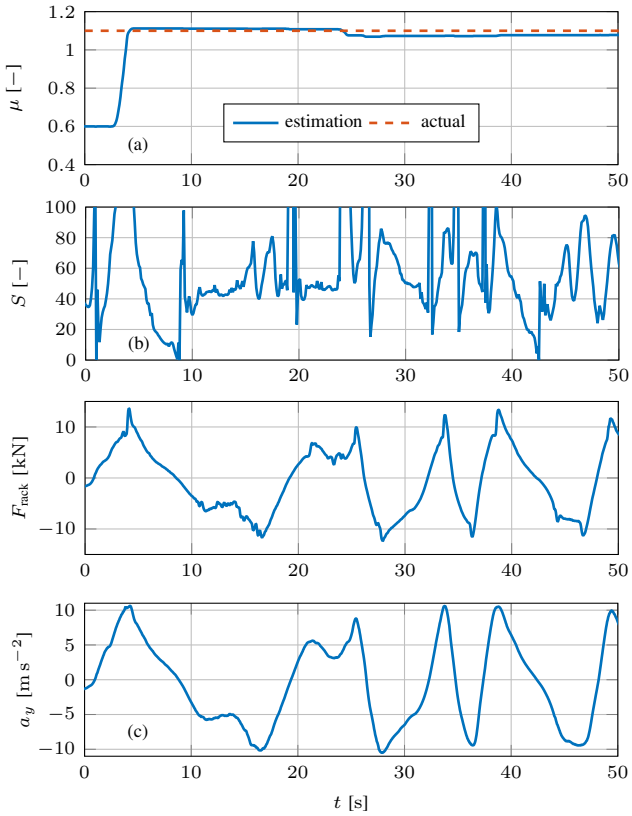

Fig. 7: Results using test rig data.

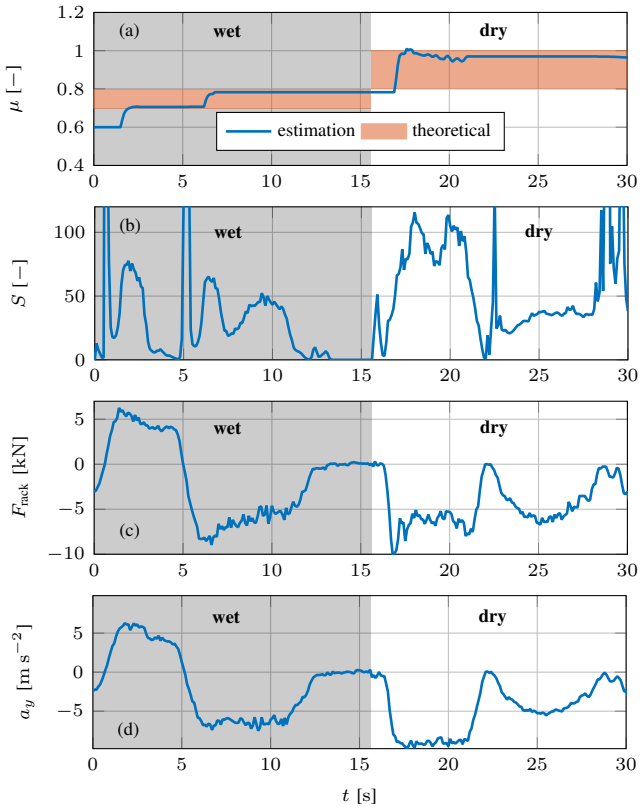

Fig. 8: Results using vehicle data during a transition from wet to dry road.

REFERENCES

[1] C.-G. Wallman and H. Åström, "Friction measurement methods and the correlation between road friction and traffic safety: A literature review," 2001.

[2] S. Müller, M. Uchanski, and K. Hedrick, "Estimation of the maximum tire-road friction coefficient," *Journal of Dynamic Systems, Measurement, and Control*, vol. 125, no. 4, pp. 607–617, 2003.

[3] D. Paul, E. Velenis, F. Humbert, D. Cao, T. Dobo, and S. Hegarty, "Tyre–road friction μ-estimation based on braking force distribution," *Proc. of the Institution of Mechanical Engineers, Part D: Journal of Automobile Engineering*, vol. 233, no. 8, pp. 2030–2047, 2019.

[4] L. Shao, C. Jin, C. Lex, and A. Eichberger, "Robust road friction estimation during vehicle steering," *Vehicle System Dynamics*, vol. 57, no. 4, pp. 493–519, 2019.

[5] T. Matsuda, S.-i. Jo, H. Nishira, and Y. Deguchi, "Instantaneous estimation of road friction based on front tire SAT using Kalman filter," *SAE International Journal of Passenger Cars - Mechanical Systems*, vol. 6, no. 2013-01-0680, pp. 147–153, 2013.

[6] Y.-H. J. Hsu, S. Laws, C. D. Gadda, and J. C. Gerdes, "A Method to estimate the friction coefficient and tire slip angle using steering torque," ser. ASME International Mechanical Engineering Congress and Exposition, vol. Dynamic Systems and Control, Parts A and B, 2006, pp. 515–524.

[7] M. Wielitzka, M. Dagen, and T. Ortmaier, "Sensitivity-based road friction estimation in vehicle dynamics using the unscented Kalman filter," in *Proc. of 2018 IEEE ACC*, 2018, pp. 2593–2598.

[8] F. Snobar, A. Michalka, M. Horn, C. Strohmeyer, and K. Graichen, "Rack force estimation from standstill to high speeds by hybrid model design and blending," in *Proc. of 2023 IEEE ICM*, 2023, pp. 1–6.

[9] J. Schäfer and R. Leidhold, "Steer-by-Wire: Eine analytische Beurteilung von unterschiedlichen Zahnstangenkraftschätzungen im Fahrzeug (German)," *at-Automatisierungstechnik*, vol. 69, no. 1, pp. 65–72, 2021.

[10] J. Dornhege, S. Nolden, and M. Mayer, "Steering torque disturbance rejection," *SAE International Journal of Vehicle Dynamics, Stability, and NVH*, vol. 1, no. 2017-01-1482, pp. 165–172, 2017.

[11] D. Schramm, M. Hiller, and R. Bardini, *Vehicle Dynamics: Modeling and Simulation*. Springer Berlin, Heidelberg, 2014.

[12] M. Ersoy and S. Gies, *Fahrwerkhandbuch: Grundlagen – Fahrdynamik – Fahrverhalten– Komponenten – Elektronische Systeme – Fahrerassistenz – Autonomes Fahren– Perspektiven*. Springer Vieweg, 2017.

[13] J. Zuurbier and P. Bremmer, "State estimation for integrated vehicle dynamics control," in *Proc. of AVEC '02*, 2002.

[14] T. Englert, A. Völz, F. Mesmer, S. Rhein, and K. Graichen, "A software framework for embedded nonlinear model predictive control using a gradient-based augmented Lagrangian approach (GRAMPC)," *Optimization and Engineering*, vol. 20, pp. 769–809, 2019.

[15] J. B. Rawlings, D. Q. Mayne, and M. Diehl, *Model Predictive Control: Theory, Computation, and Design*. Nob Hill Publishing Madison, WI, 2017, vol. 2.

[16] E. Walter and L. Pronzato, *Identification of Parametric Models from Experimental Data*. Springer, 1997, vol. 1, no. 2.

[17] T. Quaiser and M. Mönnigmann, "Systematic identifiability testing for unambiguous mechanistic modeling–application to JAK-STAT, MAP kinase, and NF-κ B signaling pathway models," *BMC Systems Biology*, vol. 3, no. 1, pp. 1–21, 2009.